Global Change Biology (2005) **11,** 1537–1555, doi: 10.1111/j.1365-2486.2005.001003.x

Characterizing interannual variations in global fire calendar using data from Earth observing satellites

CÉSAR CARMONA-MORENO*, ALAN BELWARD*, JEAN-PAUL MALINGREAU†, ANDREW HARTLEY*, MARIA GARCIA-ALEGRE*, MIKHAIL ANTONOVSKIY‡, VICTOR BUCHSHTABER§ and VICTOR PIVOVAROV§

*European Commission, Joint Research Centre, Global Vegetation Monitoring Unit, Institute for Environment and Sustainability, TP. 440, 21020 Ispra (VA), Italy, †European Commission, Joint Research Centre, SDM85, Brussels, Belgium, ‡Institute of Global Climate and Ecology, 107258, Moscow, st. Glebovskaya 20-b, Russia, §National Russian Research Institute of Physical-Technical and Radiotechnical Measurements, 141570 Moscow region, Solnechnogorsky raion, p.Mendeleevo, Russia

Abstract

Daily global observations from the Advanced Very High-Resolution Radiometers on the series of meteorological satellites operated by the National Oceanic and Atmospheric Administration between 1982 and 1999 were used to generate a new weekly global burnt surface product at a resolution of 8 km. Comparison with independently available information on fire locations and timing suggest that while the time-series cannot yet be used to make accurate and quantitative estimates of global burnt area it does provide a reliable estimate of changes in location and season of burning on the global scale. This time-series was used to characterize fire activity in both northern and southern hemispheres on the basis of average seasonal cycle and interannual variability. Fire seasonality and fire distribution data sets have been combined to provide gridded maps at 0.5° resolution documenting the probability of fire occurring in any given season for any location. A multiannual variogram constructed from 17 years of observations shows good agreement between the spatial–temporal behavior in fire activity and the 'El Niño' Southern Oscillation events, showing highly likely connections between both phenomena.

Keywords: El Niño southern oscillation (ENSO), fire activity seasonal cycle, global burnt surfaces time series, global fire dynamics

Received 10 July 2004; revised version received 12 January 2005 and accepted 2 March 2005

Introduction

Fires occur naturally and recurrently in a number of ecosystems (e.g. boreal forests, shrublands, grassland savannahs), although they can also be set by humans; elsewhere, fire is very seldom natural and usually the result of anthropogenic activity (e.g. the humid tropical forests); in yet other ecosystems it is rare altogether (e.g. peat swamp forests), and in others nonexistent (e.g. the fuel-less arid deserts). But generally speaking if there is fuel to burn and people, or natural events (such as lightning strikes) to cause ignition, fires will occur and fire remains one of the major agents of disturbance on a global scale (Thonicke *et al*., 2001). Many societies use fire as a land-management tool, with vegetation fires being set by humans for reasons ranging from forest land clearance to burning agricultural waste, from management of grazing lands to hunting (Andreae, 1991; Huggard & Gomez, 2001). The growing human population and the associated exploitation of natural resources means that fires of anthropogenic origin are unlikely to decline (Tilman *et al*., 2000), and an increase in vegetation fires is often cited as one consequence of global warming (IPCC, 2000). Indeed, the climate anomalies associated with the Southern Oscillation events have already been linked to changes in fire patterns (Malingreau *et al*., 1985; Swetnam *et al*., 1990). Furthermore, the fires themselves, whether natural or anthropogenic, have pronounced climate forcing effects. They load the atmosphere with black and organic carbon, mineral ash and volatile organic compounds, as well as greenhouse gases such as nitrous oxide, carbon dioxide and methane (Crutzen *et al*., 1979; Dignon & Penner, 1991; Galanter *et al*., 2000).

Correspondence: César Carmona-Moreno, fax + 39 0332 789073, e-mail: cesar.carmona-moreno@jrc.it

Carbon dioxide emissions from fires occurring in some ecosystems (e.g. savannah grasslands) have little impact on the long-term trend of atmospheric CO_2 concentration because a similar amount of CO_2 is sequestered in the following year's vegetation regrowth, at least in the absence of major interannual changes in biomass (Andreae, 1991; Crutzen & Carmichael, 1993). However, other ecosystems, such as forests and woodlands do not regrow so soon, and therefore the CO_2 emitted alters atmospheric concentrations for decades, even centuries (Amiro *et al*., 2001a, b; Hicke *et al*., 2003). In both savannah and forest fires, emitted products, other than CO_2, can remain in the atmosphere for a long period (Crutzen *et al*., 1979; Galanter *et al*., 2000), thus exacerbating the greenhouse effect.

Regular monitoring of global burnt surface (GBS) areas has been identified as an essential climate variable by the Global Climate Observing System (GCOS, 2003) because vegetation fires are important drivers of climate, indicators of possible climate change and have a role to play in climate change adaptation and mitigation strategies. The GCOS's requirements include the need to identify areas around the globe affected by fire, monitoring the occurrence/seasonality of fire activity and interannual variability as well as estimating the spatial distribution of burnt surfaces. Accurate descriptions of changes in fire seasonality, frequency, intensity, severity, size, rotation period and changes in fire return interval are also needed for ecological studies (Payette, 1992) because these factors have a strong influence on plant species composition (Thonicke *et al*., 2001).

Unfortunately, suitable long-term, globally consistent records of global fire activity do not yet exist. Global estimates of burnt areas have been generated from national and international statistics (Seiler & Crutzen, 1980; Hao & Liu, 1994; FAO, 2001a, b), and others have generated regional and global fire disturbance products from Earth observing satellites (Dwyer *et al*., 2000; Arino *et al*., 2001; Duncan *et al*., 2003). However, these data sets do not span long periods; the statistics studies characterize the conditions in individual years, the satellites are currently limited to a maximum of around 6 years' observations; Arino *et al*. (2001) worked with satellite images from July 1996 to February 2002, Dwyer *et al*. (2000) based their studies on remote-sensing data from April 1992 to March 1993, Duncan *et al*. (2003) worked with the Arino *et al*. (2001) data set combined with satellite based aerosol estimates made between November 1978 to May 1993 and July 1996 to present. More regular production of fire disturbance products has begun (Justice *et al*., 2002, Tansey *et al*., 2004), but these products only date from 2000 onwards and a consistent, global, longer-term perspective is still lacking.

This paper aims to characterize the variations in location and timing of fire events on the global scale over a 17-year period, spanning 1982–1999 using daily observations from the Advanced Very High Resolution Radiometer (AVHRR) on the series of meteorological satellites operated by the National Oceanic and Atmospheric Administration (NOAA).

Materials and methods

Multiannual satellite observations

The NOAA series of polar orbiting satellites have been in continuous operation since 1978, although the failure of the NOAA 13 satellite introduces a gap in 1994. From 1979 onwards the AVHRRs on-board the odd numbered (daytime overpass of around 14:30 hours local solar time) NOAA satellites record data at a nominal resolution of 1 km in five spectral channels. The channels and their center wavelengths are channel 1 (red, 0.6 μm), channel 2 (near infrared, 0.9 μm), channel 3 (shortwave-infrared, 3.7 μm), channel 4 (thermal-infrared, 11 μm) and channel 5 (thermal-infrared, 12 μm). Daily global data, sampled from the full resolution to a nominal resolution of 4 km, the so-called Global Area Coverage (GAC) product, have been archived since NOAA 7 entered service in 1981. In the 1990s, the National Aeronautic and Space Administration (NASA) began reprocessing the entire GAC Archive to create the NASA AVHRR GAC Pathfinder data set (James & Kalluri, 1994).

The Pathfinder AVHRR Land (PAL) data set consists of all five AVHRR channels mapped into the Goode Interrupted homolosine projection (equal area) at a spatial resolution of 8 km. Atmospheric corrections for Rayleigh and ozone correction are applied (Gordon *et al*., 1988). Channels 1 and 2 are calibrated using coefficients established through postlaunch vicarious calibration campaigns (Rao *et al*., 1993) and channels 3–5 are calibrated on-board (Kidwell, 1995). The complete PAL time-series covers the period from July 1981 onwards (with a gap in 1994).

Inter- and intrasatellite calibration of the AVHRRs is critical if data from all satellites in the NOAA series and throughout the lifetime of any given satellite are to be used: we want to interpret differences in measurements in terms of surface dynamics, not instrument performance. In addition to calibration issues, users of long time-series of data collected by the NOAA satellites must take orbital drift into account. The orbits of each NOAA afternoon pass satellite are known to drift to later local solar times, and this drift gradually accelerates with time in orbit. During the first year postlaunch the initial drift is slow, being on average

0.89 min per month (Price, 1991). The difference between the first and last year of satellite operation, however, can be as much as 2 h 30 min. Because the reflectance characteristics of most surfaces, including vegetation, are anisotropic this drift influences the subsequent radiance values recorded by the sensor as a result of the changing sun-target-sensor geometry.

The Pathfinder data set includes instrument calibration steps but persistent calibration problems arising from postlaunch shifts in sensor performance and continued orbital precession to later local overpass times show significant degradation in data quality from 1999 onwards and led NASA to suspend processing of the Pathfinder data set on 30 September 2001 (http://daac.gsfc.nasa.gov/CAMPAIGN_DOCS/LAND_BIO/AVHRR_News.html, last accessed 6 December 2004), and calibration uncertainties are still greater than climate change signals that may be apparent in the data (Guenther *et al*., 1997). Just as problematically, the data set includes no bidirectional reflectance distribution function (BRDF) corrections. Later attempts to introduce bidirectional corrections for AVHRR time-series over Canada have met with some success (Cihlar *et al*., 1998) although the work concludes that the tools for complete characterization of bidirectional effects are currently unavailable. Gutman (1999) followed a similar approach in analyzing 12 years' of GAC coverage from NOAAs 11 and 14 for the whole globe; new corrections for calibration drift and for solar zenith angle offered apparent improvements to the AVHRR channels 1 and 2 time-series but still left the author concluding, much like Cihlar *et al*. (1998) that while the potential to improve the available AVHRR data set exists there are still many uncertainties, especially concerning solar zenith angle corrections.

The GAC time-series is the *only* consistent, long-term global set of satellite observations from which fire information can be extracted, so the approach we have adopted here is to model likely impacts of the data set's shortcomings on GBS mapping. The PAL time-series used here includes 3 years 1 month of data from NOAA 7, 3 years 10 months NOAA 9, 5 years 10 months NOAA 11 and 5 years data from NOAA 14.

Effects of orbital precision and instrument calibration changes. To determine how orbital drift (or differences in the sensitivity of the AVHRRs on the various satellites) affected the temporal stability of the PAL data we examined the entire time-series over a stable target: the Libyan Desert test site located at 21.0–23.0°N latitude and 28.0–29.0°E longitude. This site is described by Brest & Rossow (1992) and was previously used by NOAA for their postlaunch calibration of channels 1 and 2 (Rao *et al*., 1993).

Figure 1 shows AVHRR channels 1 and 2 values from the Libyan Desert test site for the entire PAL time-series; Fig. 2 shows corresponding values from the various AVHRRs' channel 3. Channels 1 and 2 reflectance values gradually increase by up to 5% during the operational lifetime of each satellite and some differences – in the order of 1% – are seen between the different satellites in the series. The exception is the data from end of 1999 where variation is much higher (again confirming NOAAs recommendation not to use these data). The channel 3 values vary by over 5 K over the entire time-series. A decrease of less than 2 K is apparent for each individual satellite in the series, with the obvious exception of the last set of values. The large jump of over 4 K between 1993 and 1995 is probably because of a shift in gain on the sensor flying on the last satellite in the NOAA series.

We recognize that the variations of around 5% reflectance detected in channels 1 and 2 of the PAL time-series are a potential source of error but because we lack suitable tools for BRDF correction we left these values unchanged. However, for channel 3 the variations in the Pathfinder data set were too great to ignore. To correct the trends detected in the channel 3 time-series we assume that the degradation of the orbit and any degradation in sensor performance during the first year

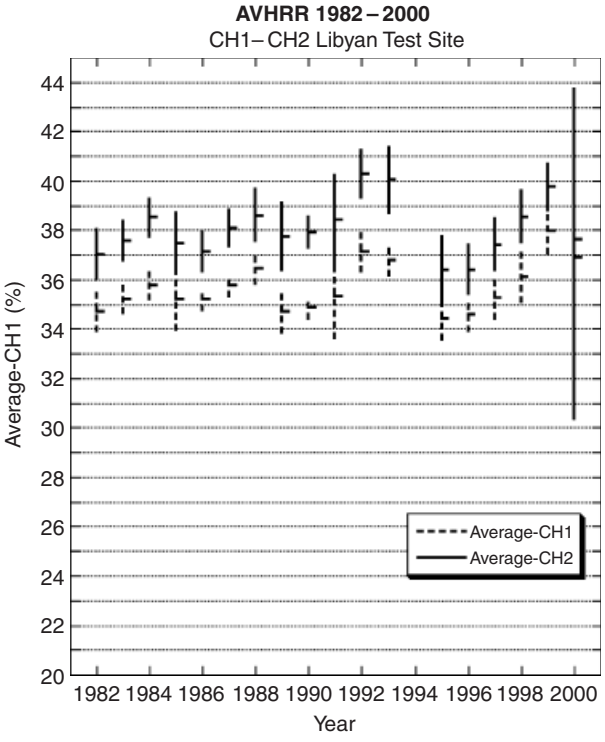

Fig. 1 Advanced Very High Resolution Radiometer (AVHRR) CH1 and CH2 average values (% reflectance) for the Libyan Test site for the period 1982–2000.

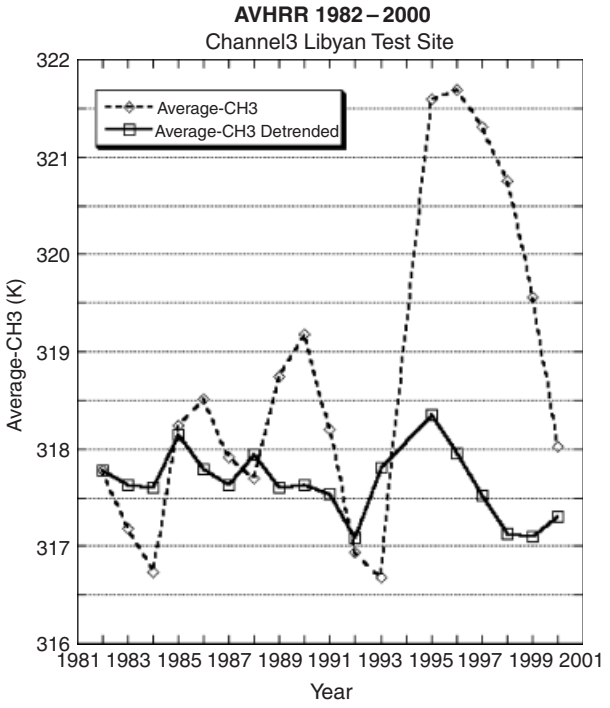

Fig. 2 Advanced Very High Resolution Radiometer (AVHRR) CH3 and CH3 detrended average values (degrees Kelvin) for the Libyan Test site in the period 1982–2000.

postlaunch are negligible, and we made a linear adjustment to the time-series using the first year's measurements as an anchor (i.e., using a moving average with 1 year lag). Figure 2 also shows the resulting 'detrended' channel 3 values.

The GBS Time-Series

Using the daily PAL data set to the end of 1999 as input (original PAL channels 1 and 2 values, detrended channel 3 values) we generated a new weekly product to monitor multiannual fire activity (Moreno-Ruiz *et al.*, 1999). The metric we use is burnt area, measured in km^2, and the final product is referred to as the GBS data set.

The algorithm for identifying burnt surfaces uses data recorded by the AVHRRs' channels 1–3 and is an extension of the approach used by Barbosa *et al.* (1999a, b). The algorithm consists of the sequential application of a series of tests applied to a 7-day minimum value composite (Barbosa *et al.*, 1998). The minimum value composite is created by retaining 1 day's channels 1–3 values for each geographic location selected on the basis of the minimum albedo value detected during the 7-day period; the albedo being computed according to Taylor (1990)

$$\text{Albedo} = 0.347\,\rho(\text{channel 1}) + 0.650\,\rho(\text{channel 2}) + 0.0746, \quad (1)$$

where ρ(channel 1) and ρ(channel 2) are the Top of Atmosphere (ToA) reflectance in channel 1 and channel 2 respectively.

The creation of minimum value albedo composites eliminates pixels with a high albedo associated with bright cloud tops, and is thus an approximate cloud-screening process that is combined with the CLAVR index of the data. Burnt surfaces are then identified from these composites by exploiting the difference in the spectral response over time of burned and unburned vegetation at the wavelengths recorded by the channels 1, 2 and 3. Vegetation indices combining reflectance measurements at red and near-infrared wavelengths are widely used to detect the presence and growth of vegetation. For this purpose the GBS uses the Global Environmental Monitoring Index (GEMI) proposed by Pinty & Verstraete (1992). Burned surfaces are usually darker (and warmer) than surrounding unburned surfaces (Belward *et al.*, 1993); a linear combination of the AVHRR channels 2 and 3, VI3T is used to emphasize this difference. VI3T is a modified version of Vi3 (Kaufman & Remer, 1994) where the reflective part of channel 3 is replaced by the full channel 3 brightness temperature (B_{T3}). The sequence and thresholds of the test follows:

$$(\rho(\text{channel 2}) < 0.125)\ \text{AND}$$
$$(\rho(\text{channel 3}) > 312.0)\ \text{AND}$$
$$(\text{Vi3t} < -0.34)\ \text{AND}$$
$$(\text{Max (GEMI)} > 0.39),$$

where Vi3t and GEMI are defined as follows:

$$\text{Vi3t} = \frac{(\rho(\text{channel 2}) - B_{T3}/1000)}{(\rho(\text{channel 2}) + B_{T3}/1000)},$$

$$\text{GEMI} = \eta(1 - 0.25\eta) - (\rho(\text{channel 1}) - 0.125) \times (1 - \rho(\text{channel 1})),$$

where

$$\eta = (2(\rho(\text{channel 2})^2 - \rho(\text{channel 2})^2) + 1.5\rho(\text{channel 2}) + 0.5\rho(\text{channe 1}))/ \times (\rho(\text{channel 2}) + \rho(\text{channel 1}) + 0.5)$$

and B_{T3} is the brightness temperature of AVHRR channel 3 and ρ(channel 3) is the ToA reflectance of AVHRR channel 3. Max (GEMI) is defined as the maximum value of the weekly GEMI data for any given pixel location.

This 'Fixed Test' is then followed by a 'Temporal Test' which uses thresholds detecting the temporal coherence of the detection on a week-by-week basis.

$$(\text{Vi3t}_w < \text{Vi3t}_{w-1})\ \text{AND}$$
$$(\text{GEMI}_w < \text{GEMI}_{w-1})\ \text{AND}$$
$$(\rho(\text{channel 3})_w > \rho(\text{channel 3})_{w-1}),$$

where $w \in [0, \ldots, 52]$ and is the current week being analyzed by the algorithm and $w-1$ is the precedent week.

A third step is then an 'Automatic Test', which takes into account the annual standard behavior (defined by the mean value of the year (m) and its standard deviation (SD)) of each pixel's radiometry. This test uses only Vi3t values given its better performance when compared with other AVHRR indices and channels (Barbosa *et al*., 1999a, b).

$$(\mathrm{Vi3t}_w < \mathrm{Vi3t}(m) - \mathrm{LCC}\,\mathrm{Vi3t}\,(\mathrm{SD})),$$

where $\mathrm{LCC} \in [1, 2]$. LCC can either be 1 or 2 depending on the land cover class. Land cover class with low fire ignition probability is equal to 2 (Evergreen Broadleaf Forests, Bare and Mosses and lichens as defined by De Fries *et al*. (1998)) all other land cover classes are equal to 1.

Because an entire year's data are needed for this test we had to exclude partial observations from the end of 1981 and 1994, hence our GBS time-series begins 1982 and 1994 is missing. Thus, we generated a multiyear GBS product spanning the period 1982–1999 where burn scars are reported each 7 days for each year.

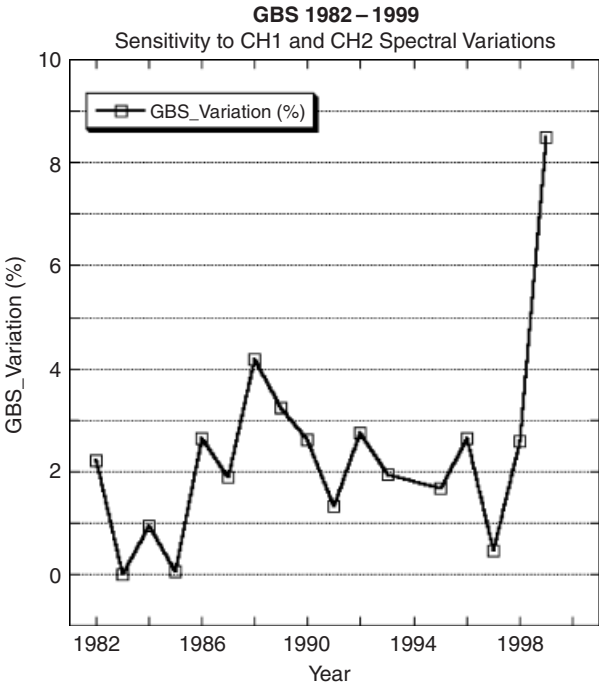

Fig. 3 Sensitivity of global burnt surface (GBS) 1982–1999 to CH1 and CH2 spectral variations.

Quality assessment

Sensitivity tests. Figures 1 and 2 clearly show that the PAL time-series is not stable over time; systematic trends of increasing reflectance during the life-time of each satellite are clearly visible. The amplitude of the variation in the detrended channel 3 values over the entire time-series is less than 1.5 K (less than 0.5% of the channel 3 sensors' range). The amplitude of the variation in the channels 1 and 2 original PAL data, as used to generate the GBS, is at least an order of magnitude greater, being 5%. As a first step in our quality assessment process, we model the effects of these channel 1 and 2 changes on the performance of the GBS algorithm.

Figure 3 represents the sensitivity of GBS algorithm to the variability of channels 1 and 2 as detected over the period 1982–1999. This is computed from the spectral variations of the channel 1 and 2 deduced from the Libyan test site. These spectral variations are introduced into the AVHRR channel 1 and 2 raw data and the GBS algorithm is run. The y-axis of Fig. 3 represents the absolute variation (%) of the GBS data as a result of the variation of the inputs (channel 1 and 2), and it also shows that there are undeniable changes over the time-series, but that these are at worst 4.2% (1988) sometimes negligible (0.04% in 1985) with the exception of 1999 when we see a variation of around 8.5%. On average across the full time-series, we see a variation of ca. 2.3%. This undoubtedly compromises the use of these data for quantitative estimation of burnt area, but the lack of any systematic trend in the sensitivity of the GBS algorithm to residual calibration errors (and the average error of around 2.3%) gives us confidence that meaningful comparisons may be made in fire activity across the time-series as a whole.

GBS 1982–1999 verification. The algorithm used to generate the GBS was developed primarily for detecting burn scars in Africa. To test how well the algorithm performs for other geographical regions we have tested the GBS data set against previously published information concerning major fire events (e.g. Potter *et al*., 2003). In total, we examined 28 exceptional events occurring throughout the time-series, sampling all ecosystems and latitude belts. Results are presented in Table 1.

In each case, we compared the season of occurrence, location and extent as reported in the literature with the season, location and size as recorded by GBS. This process does not allow a statistically based pixel-by-pixel comparison, so we cannot report percentage errors of omission (i.e. missed fire events) and commission (i.e. areas identified as fire, but not actually fire). We can, however, make qualitative comparisons. The timing and location of fire scars as detected in GBS and as previously published agreed in

Table 1 List of large referenced wildfires over the period 1982–1999

Num.	Location	Period	Latitude/Longitude	Reference	Agreement with global burnt surface (GBS)
1	Kalimantan	November 1982–April 1983	8°N–4°S/107–119°E	Goldammer & Hoffmann (2001)	Good
2	Ivory Coast	December 1982–March 1983	7°N/5°W	Oura (1999)	Good
3	Australia	December 1983	24°S/134°E (Alice Springs)	Allan & Southgate (2002)	Good
4	Australia	1985	24°S/134°E (Alice Springs)	Allan & Southgate (2002)	Good
5	China–Russia	May–June 1987	44–55°N/120–135°E	Cahoon *et al.* (1991)	Good
6	Yellowstone Park	Summer 1988	44.6°N/110.7°W	Romme & Despain (1989)	Good
7	Alaska	May–August 1990	60–64°N/140–155°W	Boles & Verbyla (2000); Kasischke *et al.* (1995)	Very Poor – period of the year detected but underestimation (<20%)
8	Alaska	May–August 1991	60–64°N/140–155°W	Boles & Verbyla (2000); Kasischke *et al.* (1995)	Very Poor – period of the year detected but underestimation (<20%)
9	Russia	May–August 1992	45–75°N/90–150°E	Conard & Ivanova (1998); Conard *et al.* (2002); Cahoon *et al.* (1996)	Good
10	Central African Republic	Mid-October 1994–early March 1995	2–13°N/10–35°E	Eva & Lambin (1998);	Good
11	Canada	May–August 1995	50–58°N/65–100°W	Li *et al.* (2000)	Good
12	Portugal	June–October 1995	39.5–42.5°N/6–9°W	Pereira & Dos Santos (2003)	Poor Plus – over estimation because of hot surfaces in the south of Portugal (Almodovar)
13	Patagonia	September 1995–early April 1996	35–55°S/56–74°E	Cwielong (1996)	Good
14	Mongolia	February–June 1996	47–55°N/97–120°E	Shulman (1996)	Good
15	Canada	Late May–August 1996	47–58°N/65–95°W and 55–65°N/90–130°W	Li *et al.* (2000)	Good
16	Mongolia	Late February–June 1997	47–55°N/97–120°E	Erdenesaikhan & Erdenetuya (1999)	Good
17	Canada	Late May–August 1997	50–58°N/65–100°W	Li *et al.* (2000)	Good
18	Alaska	Late May–mid-August 1997	63–64°N/159°W	Boles & Verbyla (2000)	Very Poor
19	Northern Australia	May–late November 1997	11–27°S/118–152°E	Russell-Smith *et al.* (2003); Edwards *et al.* (2001)	Very Good
20	East Kalimantan	Late May 1997–early June 1998	3S–3°N/114–119°E	Siegert *et al.* (2001)	Good
21	North of South America	January–April 1998	2°S–10°N/58–73°W (in Roraima–Brazil)	Elvidge *et al.* (2001)	Very Good
22	Mongolia	Late February–early June 1998	47–55°N/97–120°E	Erdenesaikhan & Erdenetuya (1999)	Good
23	Mexico	April–May 1998	14–22°N/87–101°W	Galindo *et al* (2003)	
24	Canada	Mid-April–late October 1998	47–58°N/65–95°W and 55–65°N/90–130°W	Li *et al.* (2000); Johnston (1999)	Good
25	Russia Far East	Late May–early November 1998	40–70°N/110–145°E	Tanimoto *et al.* (2000)	Good
26	Portugal	June–October 1998	39.5–42.5°N/6–9°W	Pereira & Dos Santos (2003)	Poor Plus – over estimation because of the hot surfaces in the south of Portugal (Almodovar)
27	Sumatra	February–December 1999	3°N–6°S/98–107°E	Anderson *et al.* (2000)	Good
28	Siberia	April–August 1999	50–70°N/76–150°E	Soja *et al.* (2004)	Poor

all 28 cases, but the size of the fire event as measured in GBS and independently reported varied considerably. In Table 1, we define the agreement between previously published documents and GBS as 'Very Good', where location and timing agree and where the area estimation from GBS is between 80% and 100% of that independently documented. Agreement is judged 'Good' if location and timing agree and area estimates from the GBS are between 60% and 80% of that reported elsewhere. 'Poor' agreement is where location and timing agree but the GBS area estimate is only 20% to 50% of that reported, and 'Very Poor' agreement occurs where location and timing agree, but GBS identifies less than 20% of the area. Those areas where location and timing agree, but where GBS identifies more than 100% of the area as previously reported are judged 'Poor Plus'.

GBS over-estimated fire area in only two out of the 28 cases. Fire area was underestimated in all of the other 26 fire events we checked. Performance, in terms of fire area estimation, was particularly bad at high latitudes, which unfortunately include the extensive and fire-prone forests of the northern boreal zone-although the seasonal behavior of these fires was detected.

As an additional global check we compared the GBS maps with the monthly active fire patterns for the years 2002 and 2003 available from the Web Fire Mapper (http://maps.geog.umd.edu/products.asp; last accessed 25 November 2004). This site presents global active fire locations as detected by the Moderate Resolution Imaging Spectroradiometer (MODIS) instrument (Justice *et al*., 2002, Davies *et al*., 2004). The MODIS active fire maps again showed active fire activity in all the regions identified as containing burn scars in GBS, but showed far more widespread fire activity in high northern latitudes, again suggesting that the GBS underestimates, rather than overestimates fire activity.

From the results of the comparisons made in Table 1 and with independently published information on active fires we deem it inappropriate to use the GBS time-series as a means of comparing absolute measures of fire area across different geographical regions. However, the good agreement concerning location and timing does not compromise the use of GBS for looking at inter- and intra-annual variations in regions affected by fire and in fire calendar. And while geographical errors are undoubtedly present these too are consistent over time. The underestimation of fire activity between 40° and 70° north is certainly real, but as the same algorithm was used throughout and the input data were all uniformly treated we can assume the temporal variation to reflect (albeit sampled) genuine variations in fire activity with time at these, and indeed any other, latitudes.

Results and analysis

Fire seasons by latitude

The weekly GBS product at 8 km is the initial output. To provide a multiannual overview of global fire seasons we first summed each year's weekly data into four trimesters according to conventional seasonal groupings (December, January, February – DJF; March, April, May – MAM; June, July, August – JJA; September, October, November – SON). We then summed the 17 years record for each trimester. However, during the 17 years of our study, the trimester in which fires occur at any given location can, and does, change. For each 8 km grid cell we determine all dates at which burn scars are detected and then represent the mode. Figure 4 shows the global synthesis of all burnt areas detected over the entire time-series. The limitations of plotting individual features, such as burn scars, in global maps at very small scales, such as Fig. 4, hides (or blurs) much detail. Figures 5 and 6 complement the map and are included as a means of showing the seasonal behavior in more detail. These show the cumulative burnt area for each trimester/season, and the total, as a function of latitude. Note, that in Fig. 5 all burnt areas have been normalized to the absolute peak in fire activity, in Fig. 6 the relative contribution of each season's burning for each degree of latitude is shown.

Fire season probability maps

Another important aspect in defining the global fire regime (Payette, 1992) is the probability of fire occurring in a particular season for any given area (latitude i, longitude j). This can be described as the probability for a given area at latitude i, longitude j to burn in a given unit of time. Here, we consider that the unit of time is a trimester and a unit area is a $0.5^\circ \times 0.5^\circ$ latitude–longitude cell. This is formally defined by:

$$P(\mathrm{BS}p_{(i,j)}) = \frac{\sum_m \mathrm{BS}p_{(i,j)}}{\sum_{p=1}^{p=4} \sum_m \mathrm{BS}p_{(i,j)}}, \qquad (2)$$

where $P(\mathrm{BS}p_{(i,j)})$ is the probability of a $0.5^\circ \times 0.5^\circ$ cell (latitude i and longitude j) to burn in a trimester p of the year; $\sum_m \mathrm{BS}p_{(i,j)}$ is the number of burned pixels detected in the cell (i,j) for the trimester p of the year ($p = \{1,2,3,4\}$); where m is the number of pixels (8 km) in the $0.5^\circ \times 0.5^\circ$ cell and $\sum_{p=1}^{p=4} \sum_m \mathrm{BS}p_{(i,j)}$ is the total number of burned pixels detected in the cell (i,j) along the 17 years considered in this paper.

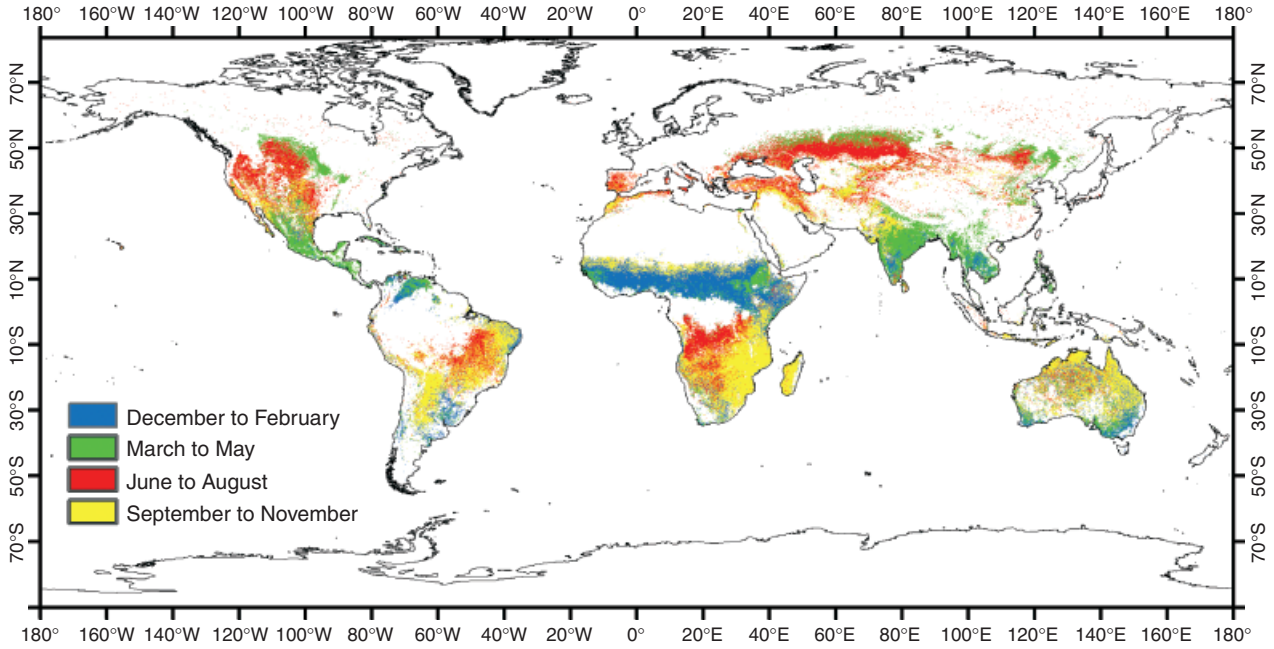

Fig. 4 Global fire activity seasonal cycle. This figure represents the seasonal distribution of the fire activity obtained from the accumulated spatial–temporal distribution of the global burnt surface products for the period 1982–1999.

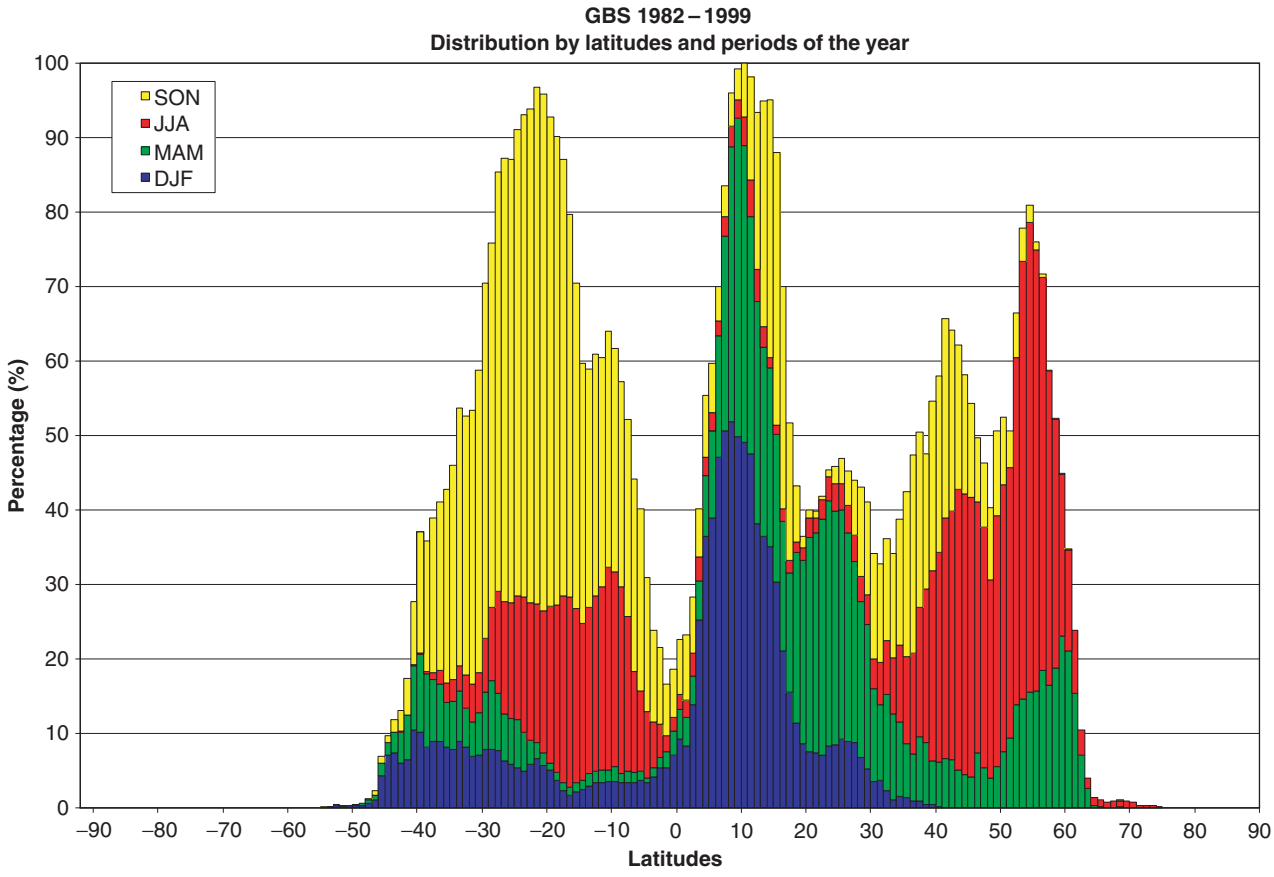

Fig. 5 Accumulated and normalized fire activity distributed by latitudes for the period 1982–1999.

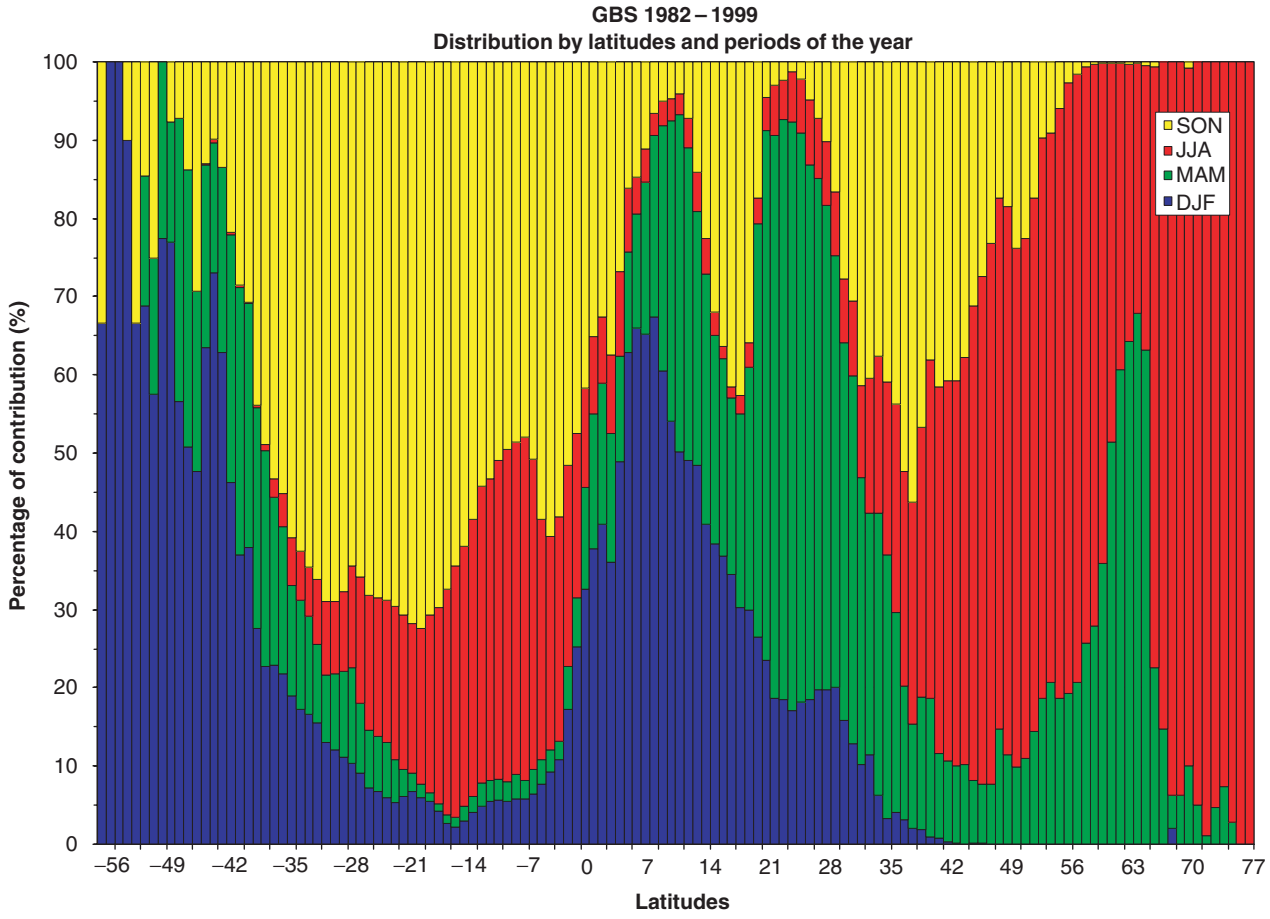

Fig. 6 Contribution of burned surface (considered as a proxy of the fire activity) for each trimester of the year per latitude.

The outputs of this computation are four fire season probability maps (one per trimester). These are shown in Fig. 7(a)–(d). By definition, the sum of the probabilities of the four periods is equal to 100% for those regions where the total number of burned pixels is not equal to 0 (no fire detected during the 17 years time-series) in order to have a homogenous system.

We can see for instance the low probability of fire occurring in the first trimester of the year (winter) in the Mediterranean area and/or in high latitudes of the boreal region. The probability strongly increases during the second and third periods of the year (this point will be further discussed in the Results). Peaks of probability occur in trimesters of the year in those latitudes where fire activity reaches its maximum.

Characterizing multiannual patterns in fire occurrence

To model the spatial–temporal structure of the data for the entire 17 years time-period, we constructed a variogram of the GBS time-series. The variogram can be considered as a quantitative descriptive statistic that can be graphically represented in a manner that characterizes the spatial and temporal continuity of the data analyzed. The mathematical definition of the variogram is:

$$\gamma(\Delta x, \Delta y) = \tfrac{1}{2}\varepsilon\left[\{Z(x+\Delta x, y+\Delta y) - Z(x,y)\}^2\right], \qquad (3)$$

where $Z(x,y)$ is the value of the variable of interest at location (x,y) and $\varepsilon\frac{1}{2}$ is the statistical expectation operator. It should be noted that the variogram, $\gamma(x,y)$, is a function of the separation between points $(\Delta x, \Delta y)$, and not a function of the specific location (x,y) (Isaaks & Srivastava, 1989).

We first took the 52 weekly global maps of burned surface for all 17 years and summed the burned surfaces by trimester and by latitude in 0.5° strips. Figure 8 shows the standardized variogram where the proportional effects (i.e. the variance value increases with the increment of the average) are removed. A quadratic trend has also been removed from the data. Removing these two elements of the data that may be considered structural perturbations does not affect the

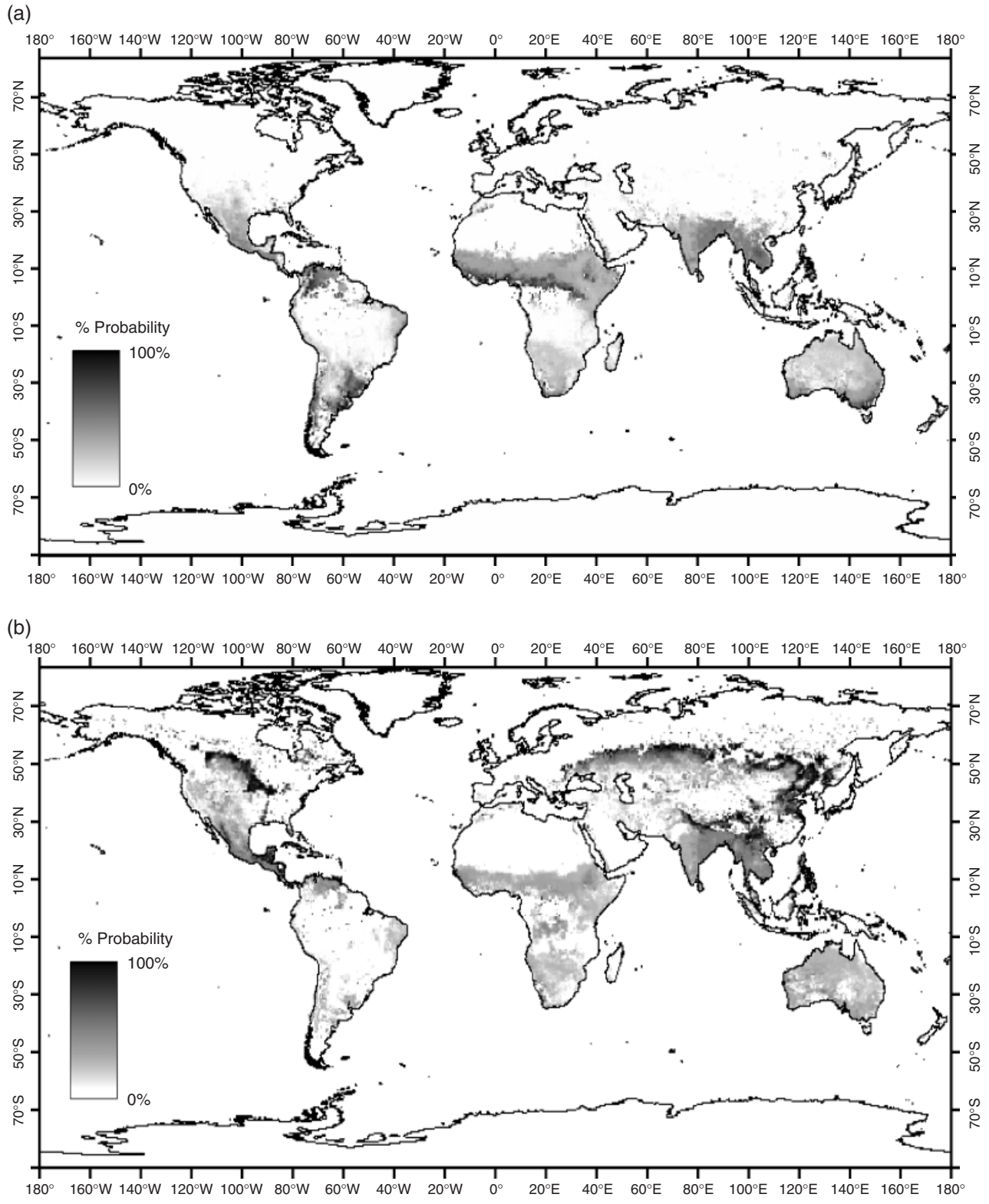

Fig. 7 Fire seasonal probability (a) December–January–February, (b) March–April–May, (c) June–July–August and (d) September–October–November.

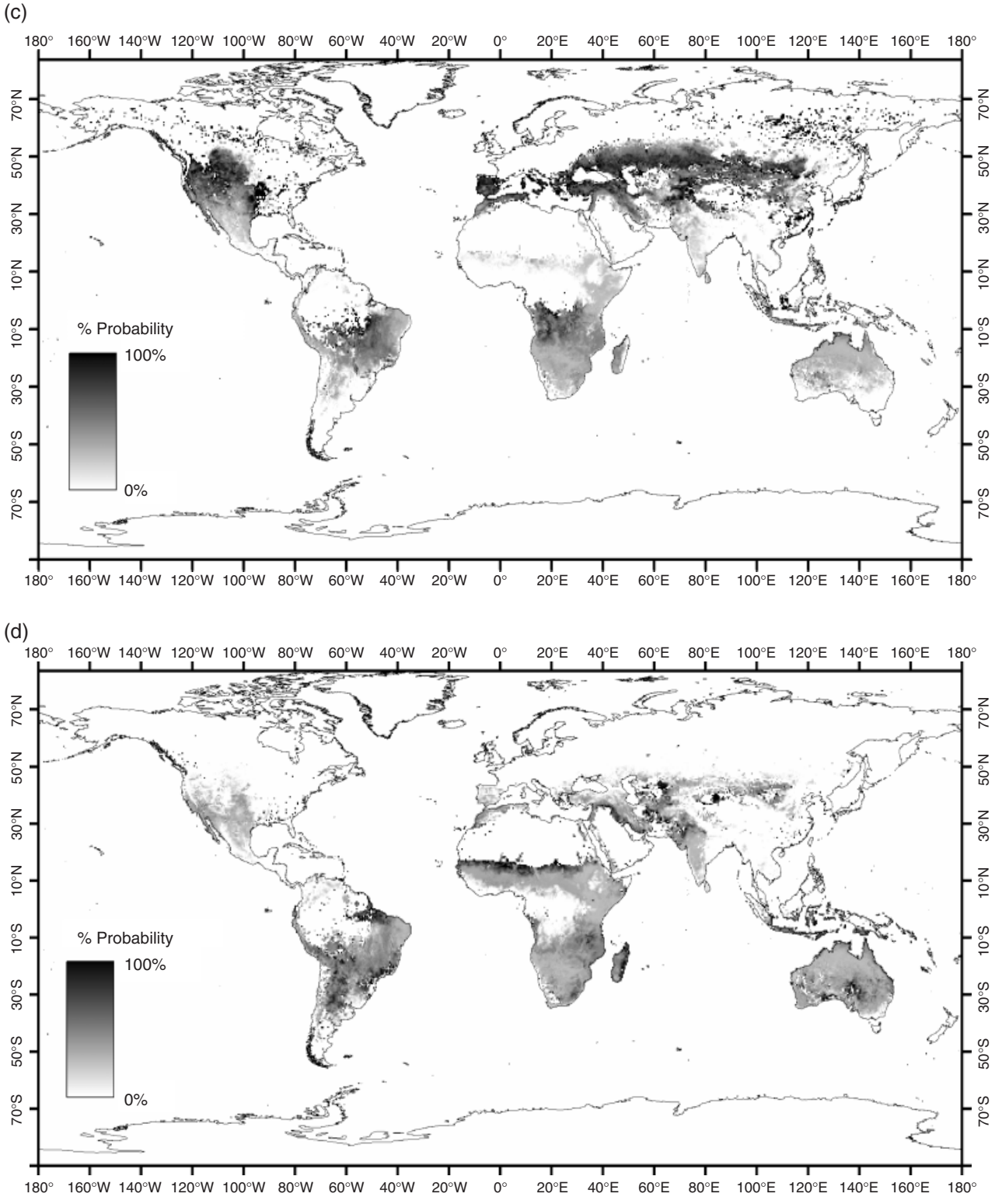

Fig. 7 Continued.

spatial–temporal structure we see. In other words the variogram is highly stable.

From the analysis of the variogram, we see that there is a low nugget effect (~30%); thus we account for close to ~70% of the spatial–temporal correlations in our time-series with this trimester-based model. We fit the data with an exponential model (scale = 1, length = 3.5 with an anisotropy defined by a ratio = 1 and angle = 0). This model shows that the range (the distance between the origin and the point at which the variogram reaches the sill (i.e., at the standardized variogram value of 1)) occurs after 16 trimesters, confirming a regular pattern in the time-series with this periodicity. In the same way, Fig. 8 also shows a pattern occurring every 4 trimesters, i.e. a strong annual periodicity.

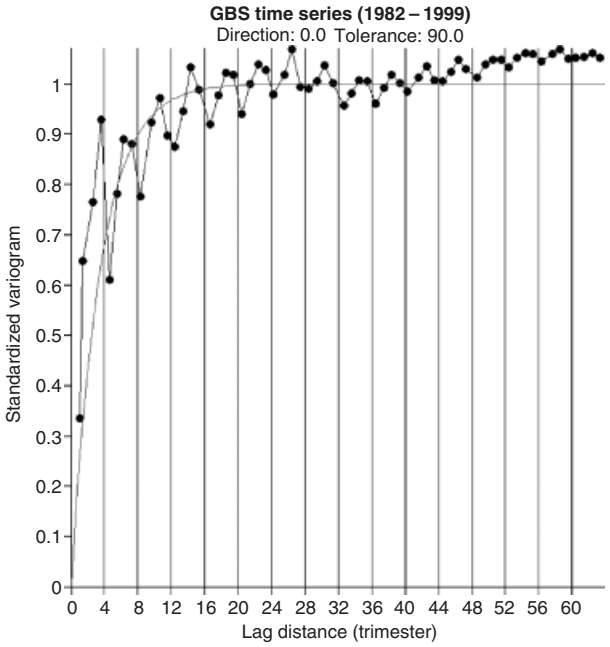

Fig. 8 Global burnt surface (GBS) time-series 1982–1999 standardized variogram.

To provide spatial representation of the variogram model a gridding method was used to fit the exponential model from the variogram to the GBS data. The result is shown in Fig. 9. This Figure shows the spatial–temporal structure of the GBS data distributed by latitudes (*y*-axis), time (*x*-axis, trimestrial periods), with burned surfaces summed during each trimester and by 0.5° of latitude. The contour interval represents 500 burned pixels.

The variogram results are supported by frequency analysis of the GBS time-series, shown in Fig. 10. This has been computed using the Fast Fourier Transform (FFT).

Results and discussion

An overview of global fire activity

The global burnt area synthesis shown in Fig. 4 conforms to previously established geographic distri-

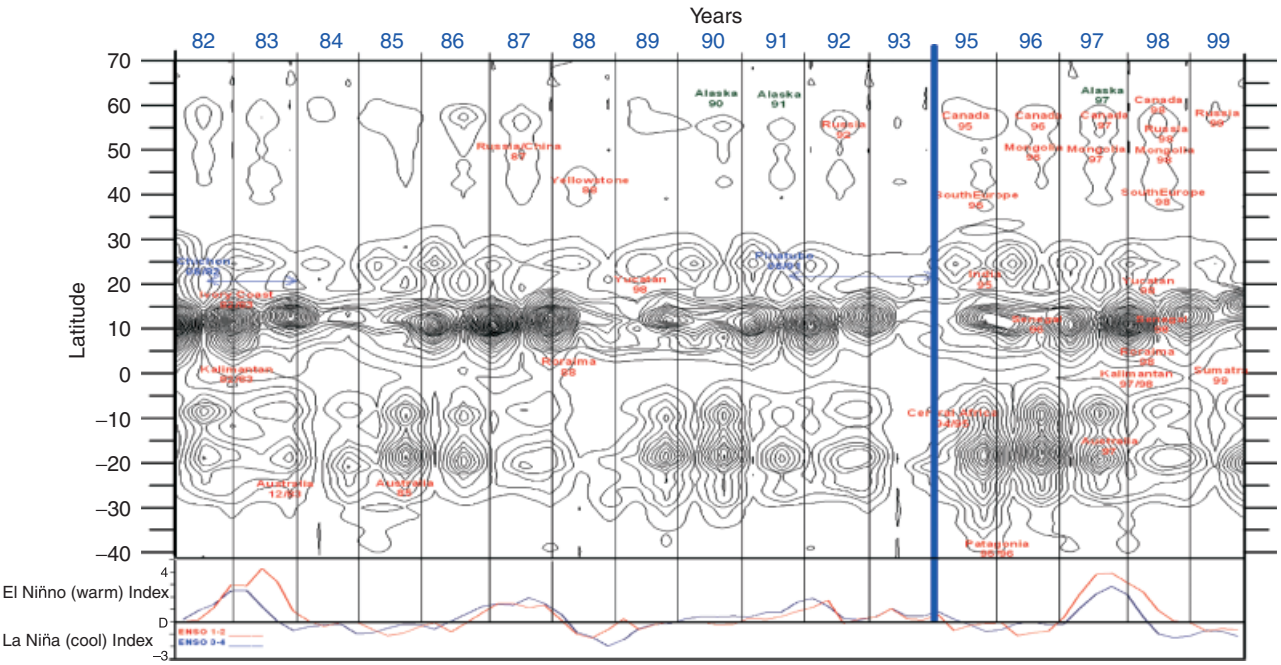

Fig. 9 Spatial–temporal distribution of global burnt surface (GBS) time-series and El Niño southern oscillation (ENSO) Index (regions 3.4 and 1–2) during the period 1982–1999. The Chichon's (08/1982) and Mount Pinatubo's (06/1991) eruptions (in blue), and main fire events (in red) occurred during the period considered in this paper are also showed.

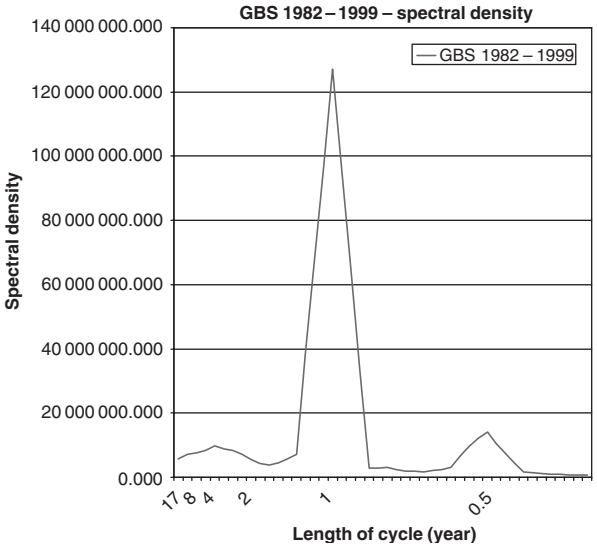

Fig. 10 Periodogram representing the frequency component of the global burnt surface (GBS) time-series.

butions (e.g., Tansey *et al*., 2004); Australia as a 'fire' continent is highly evident, the almost unbroken ring of savanna fires surrounding the largely untouched tropical forests of central Africa, the agriculture and savanna fires extending into the Amazon Basin (especially the southern fringes), the forest fires of the Mediterranean Basin, the grain producing lands, rangeland and forest fires of North America and Central Asia can all be clearly seen, as can the fires in southern Asia's forests and rice fields, and a scatter of fire scars across the boreal forests of the north. Fire is at an absolute minimum at the very high latitudes above the Arctic and Antarctic Circles. Another major gap corresponds to the moist humid tropical forests, with other marked gaps in fire activity corresponding to the barren regions, such as the Sahara, and the intensely urbanized, Eastern USA and Western/Central Europe. The global seasonal synthesis shown in Figs 5 and 6 gives further emphasis to the observation that biomass burning is a truly global and continuous phenomenon; burn scars are only absent at the very highest latitudes and fires occur during all seasons on both sides of the equator.

The northern hemisphere's fire seasons. Northern hemisphere fire activity during the months of December, January and February is principally confined to latitudes below ~35°N. Fires across Africa's northern savanna belt, agriculture and grassland burning in the Orinoco valley of Colombia–Venezuela and across southern India and South East Asia contribute to the dominant peak between ~3 and ~17°N. The fires in Africa extend throughout the grass and shrub savannas through to the fringes of the humid tropical forests, and are closely linked to the onset and advance of the dry season, mainly between October and March (Delmas *et al*., 1991). A second, less pronounced peak occurs at this time between ~17 and 35°N. This is dominated by fire activity in northern India and Asia towards the end of the trimester. Very little burning in this season occurs above 35°N, and almost nothing above 40°N.

Fire activity in March, April and May occurs throughout the northern hemisphere, although three distinct peaks do occur; one peak, occurring between ~3 and 17°N, is mainly accounted for by late dry season burning in Africa's northern savannas; a second peak between ~17 and 40°N can be accounted for by fire in the tropical pine forests of Central America and Southeast Asia – the latter are often as a result of grazing land management fires and shifting cultivation. This period also sees fires in Asia linked to the burning of rice field stubble before the onset of the moist South West Monsoon, as well as land clearance and some rangeland management fires. Tropical pine forest fires and agricultural crop residue clearing in Central America and Asia add significant amounts of burning, especially in April to June, and significant burning also occurs in India's remaining forests (from the temperate forests of the north to the tropical forests along the West Coast), which come under threat from fire each year, especially in March and April (Saha & Hiremath, 2003). Land clearance, accidental fires from shifting cultivation and fires used for the management of nontimber forest products such as mahua (*Madhuca indica*) flowers and kendu (*Diospyros melanoxylon*) leaves account for much of this activity (Jaiswal *et al*., 2002; Reddy & Venkataraman, 2002). The third peak in burning embraces the postharvest stubble clearance and crop residue fires of the agricultural regions between 45 and 55°N, the grassland and forest fires of the central Eurasian steppe and, above 60°N, early summer forest fires in the boreal zone.

Very little burning occurs in the months of June, July and August between ~3 and 30°N. However, this is the season where the Mediterranean basin and Pacific Northwestern USA experience their peak forest activity (lightning ignition from summer convective storms is a major factor; Rorig & Ferguson, 1999), and when Eurasia's more southerly steppe and forest burns. It also represents the peak period for fire activity in the boreal forests, where again lightning ignition is a significant factor (Stocks, 1991).

Northern hemisphere fire activity does occur during the autumn months of September, October, November, but is minimal above ~50°N. Below this latitude the African grasslands are a focus for much of the activity. The northernmost savannah shrub and grasslands

between ~12 and 17°N burn early in the dry season – a peak in burning occurs here between October and November – with fire activity following the advancing dry season south until reaching the humid forest margins between January and March. The fire activity between ~30 and 50°N during this period are mainly late summer (September) fires in the forests of north Africa, Central Asia and the North America – Central America confines.

The southern hemisphere's fire seasons. Although not on the same scale as in the north, southern hemisphere fire activity does occur during the months of December, January and February. This commences at the equator, but has a stronger presence at latitudes below 16°S. Australia, especially the southern half of the continent (Craig *et al.*, 2002), and South America are the main centers of fire activity at this time, although southern Africa also experiences some fire activity in these months, especially in the Cape Town region (Calvin & Wettlaufer, 2000) and South West Botswana (Brockett *et al.*, 2001; Dube, 2004). Argentina's forest fires usually occur around the month of February (Cwielong & Rodriguez, 1993), and fire activity peaks around this period in Chile too, (http://www.ine.cl/17-ambiente/catastrofes.htm – last accessed 25 November 2004).

Again, in contrast with the northern hemisphere, there is relatively little fire activity in March, April, May in the south. Most of the fires that do occur in this period occur in Australia, especially in the temperate plains and agricultural regions to the south west and south east of the continent (Williams, 2001), as well as in the more northern parts of the arid interior.

Burning in the southern hemisphere savannas of Africa and South America, combined with a marked dominance of fire in the north of Australia (Craig *et al.*, 2002) lead to the first of two peaks in southern hemisphere fire activity; this one occurring in the months of June, July and August and extending from the Equator down to ~16°S. This latitude belt embraces the deforestation arc at the southern margins of the Amazon Basin, where burning starts around July and finishes in November with a peak at the end of July/early September (Christopher *et al.*, 1998). It also encompasses the African savannas just to the south of the central African rainforest.

The second, and larger southern hemisphere peak occurs from September, through to November. This dominates the more southern latitudes, extending down from ~16 to 40°S. In Australia this period sees a general swing in fire activity to the eastern tropical costal margins and the subtropical plains. In Africa it is the more southerly savannas that burn, and in South America from the centre to the south (Pampa – Patagonia regions), the fire activity is concentrated in the summer period where the dry season occur. Below ~35°S fire activity at this time is minimal, with fires tending to occur in January to March.

Global fire calendar probability maps

In the preceding sections, we have shown that typical fire seasons exist for each geographic location on earth. Because fire is sensitive to prevailing climatic/meteorological conditions (among other factors) these seasons are not completely stationary over the 17 years record we are working with. In this section, we propose global maps showing the probability of fire occurring for any given location for each of the four seasons. Figure 7(a)–(d) shows each season's probability map, where the resolution has been degraded to 0.5° grid. These data are freely available from http://www-gvm.jrc.it/.

Figure 7 provides a spatially explicit guide as to the location and timing of fire on the global scale. This information is closely linked to temperature and precipitation, and therefore, with the prevailing climate conditions, which have direct implications on the state of the biomass including fuel amount and fuel moisture content (Camberlin *et al.*, 2001; Lyon, 2004). As we will see in the following section, climate variability induces temporal and spatial shifts in fire seasonality in different parts of the world. In other regions these shifts do not occur. This stability, and lack of it, is evident in the 17 years fire probability maps.

The fire seasons in some regions are very stable over the entire 17 years record. These are the areas in Fig. 7 that have either very high or very low probability during any particular trimester. This is the case for the high and medium latitudes in the Northern Hemisphere (JJA), Far East of China–Russia (MAM), Central Africa (JJA), and African savannas (DJF and SON). We can hypothesize that in these areas interannual variations in climate have little or no effect on fire seasonality, although of course may still influence the size, intensity and efficiency of fire. However, in other regions, even if there is always a maximum of probability in a given trimester, the peak is less evident (i.e., the timing of fire activity across the 17 years varies quite widely). Thus, in Fig. 7, we see relatively high probabilities of fire for these regions in several trimesters. This homogeneity in the temporal probability distribution can be interpreted as particularly fire prone areas/ecosystems, or areas that are more sensitive to interannual climate variability. This is the case in Indonesia, Southern Europe, Southern and East Africa, California, Australia, Southern East Asia, Central and Northern Latin America.

Interannual variability in fire calendar

Although the 17 years summary presented above substantiates the concept of typical fire seasons for specific locations across our planet, these seasons are by no means truly stationary, as indeed confirmed by the variogram in Fig. 9. This figure expands the view of global fire dynamics by presenting the area burned for each trimester of each year as a function of latitude. Size of burned area is implied by the contour spacing (level step = 500 burned pixels). The fire events reported in Table 1 have been positioned in the Figure, as have two major volcanic eruptions and the El Niño/La Niña events that occurred over this time-span. Although the data are presented year-by-year, fire seasons do not adhere to the Gregorian calendar and references to specific years/months are made to guide the interpretation; to this end January of each year is shown as a solid vertical line.

Looked at in the latitude axis, Fig. 9 shows that each year's fire distribution follows much the same pattern as described in 'An overview of global fire activity'; fires occur at most latitudes, maximum fire activity occurs between the two Tropics, least fire-prone belts are found close to the equator and between 30 and 40°N; a noticeable offset occurs in the timing between the southern and northern hemisphere burning maxima, and both hemispheres show maxima occurring at more than one time within a single year.

Yet, while strong annual periodicity (and to a lesser extent intraannual periodicity) of burning is apparent throughout the time-series, considerable interannual variation can be seen on both sides of the equator. This falls into a repetitive 4-year pattern, where the various peaks and troughs correlate well with El Niño Southern Oscillation (ENSO) events during this period.

The apparent ENSO effects on fire calendar tend to mirror each other across the equator. In the northern hemisphere El Niño periods are linked to enhanced fire activity, and fire activity gradually increases from year-to-year as these periods persist. Manzo-Delgado *et al*. (2004) have shown an increase in Central Mexico's fire activity during El Niño induced droughts, and fires in the Yucatan forests of 1989 were linked to both drought and the aftermath of Hurricane Gilbert – the storm opened up forest and provided good fuel, the drought 'cured' the fuel, and run-away land clearance fires completed the picture (Goldammer, 1992). An increase in the frequency and extent of fires across North America have been linked to large-scale climate patterns in conjunction with El Niño (Swetnam & Betancourt, 1990; Bartlein *et al*., 2003; McKenzie *et al*., 2004) and even in Europe good correlations have been found between increased fire activity and the El Niño (Rodo *et al*., 1997). Figure 9 shows that fire activity in the high northern latitudes is variable, both annually (in terms of latitudes affected) and interannually (in terms of both timing and frequency of occurrence). Figure 9 also shows that the latitudinal limits of fire in the north tend to spread further south during El Niño years. The interannual variability of burning at these latitudes and a strong agreement between the interannual peaks of activity mainly occurring during El Niño events has been reported by Conard *et al*. (2002), Li *et al*. (2000) and Soja *et al*. (2004) among others.

During La Niña periods fire activity in the northern hemisphere is not just lower, but is also more dispersed over space and time. During these periods the fire seasons are longer, less concentrated and less well defined. The peak in fire activity also occurs later in the season.

The northern hemisphere pattern of 'strong and symmetrical' fire seasons coinciding with El Niño periods and 'weaker, more dispersed' fire seasons during La Niña largely inverts in the south, at least below 5°S; fire activity is more concentrated and symmetrical during La Niña periods, more dispersed and with longer seasons during El Niño. The southern limits of the bulk of the southern hemisphere's fire activity are always greater in La Niña than El Niño periods.

Fire activity between 5°N and 5°S, as depicted in Fig. 9, is always strongest during the El Niño periods. This too, agrees well with previously published work asserting that in Indonesia, fires occur on annual basis, but unusually large fire events occur during El Niño events, particularly the devastating fire activity of the extreme 1982–1983 and 1997–1998 ENSO episodes (Malingreau *et al*., 1985; Wooster *et al*., 1998; Legg & Laumonier, 1999; Wooster & Strub, 2000; Siegert *et al*., 2001).

Two major volcanic events also occurred during the period of time considered in this study: the eruptions of El Chichon and Mount Pinatubo took place, respectively, between March 28 and April 4 1982 at 17°23′N, 93°12′W and between June 11 and 16 1991 at 15°08′N, 120°21′E. In both cases effects on Earth's climate were detected because of the enormous ejection of volcanic material into the stratosphere. This is mainly because of the sulfur dioxide (SO_2), which combined with water vapor to form droplets of sulfuric acid, effectively blocking some of the sunlight from reaching the Earth. The consequence is a cooling effect (of ca. 0.2 °C in the case of El Chichon and 0.4 °C for Mt Pinatubo), although the cooling in both cases was somewhat moderated by warming associated with ENSO events, although far less so in the case of Pinatubo (Self *et al*., 1996). The massive amounts of aerosol injected into the

stratosphere (7 million tons of SO_2 for El Chichon and 22 million tons of SO_2 for Pinatubo) certainly appear to have depressed fire activity between 15 and 30°N, but we cannot discount the fact that the atmospheric corrections used to generate the PAL data, which formed the basis of our global estimates of burnt surface, did not adequately deal with such aerosols, and so the detection itself may have been compromised.

Although largely substantiated by previously published work, we further analyzed the inter/intraannual variations in calendar shown in Fig. 10 through frequency analysis of the entire 17 years of weekly global burned surface measurements. Figure 10 shows the results of the frequency analysis of the time-series. This reveals an important yearly periodicity (i.e. confirming there is a dominant annual burning cycle); this can be attributed to the intense fire activity within the tropics linked to each hemisphere's dry season. A less important, yet quite obvious intraannual maxima can be attributed to one fire peak within the tropics and a second peak at the higher latitudes corresponding to each hemisphere's high latitude 'summer' fires. And a quadrennial component is also clearly evident; this correlates well with ENSO events, at least for the 17 years time-period analyzed here. (It is worth recalling here that the various NOAA satellites making up this PAL time-series did not operate on a 4-year cycle.)

Conclusions

From analyzing a 17 years record of satellite observations, we have shown that biomass burning is unequivocally a global scale phenomenon. We have also shown that it is a perpetual process when viewed globally, fire occurs somewhere on our planet every week, if not every day. Furthermore, this is the case for both hemispheres independently: they both burn all year round.

Through constructing a spatially explicit multiannual database documenting global burnt area we have been able to define fire seasons and probability of fire occurring within any season for all latitudes and all ecosystems. Some regions show high levels of interannual variability in burning period, others are stable: they always burn at the same time each year, regardless of shifts in the prevailing global climate. We have also converted this information into maps showing fire probability by season for every 0.5° grid-cell; these data are available from http://www-gvm.jrc.it/. In this form these data should find use for initiating and/or validating the output from dynamic vegetation models, trace gas emission models and general circulation models.

Our analysis also highlights shortcomings in the currently available processed AVHRR record and current generation of global burn scar detection algorithms. Improvements in both areas should lead to more reliable measures of actual area burned, to complement the existing capability, as reported here, concerning characterization of location and timing of major fire events.

While 17 years is not long enough to definitively identify trends in biomass burning patterns, these results do confirm a global scale influence of the ENSO phenomena on fire activity. Long-term, reliable observations of global fire activity would be a major source of information with which to fully confirm this. And we share Gutman's (1999) observation that in spite of their problems AVHRR time-series have potential for studies of medium-range response of ecosystems to various weather and climate phenomena. This paper highlights both the need for more thorough reanalysis of the GAC record to support global fire studies, and the considerable value in doing so.

Acknowledgements

We wish to thank the continuous support of the GVM Computer Service and to NASA-GODDARD DAAC for providing with NOAA-AVHRR GAC 8 km data. The comments of the anonymous reviewers are greatly appreciated.

References

Allan GE, Southgate RI (2002) Fire regimes in spinifex landscapes. In: *Flammable Australia: The Fire Regimes and Biodiversity of a Continent* (eds Bradstock RA, Williams JE, Gill AM), pp. 145–176. Cambridge University Press, Cambridge.

Amiro BD, Stocks BJ, Alexander ME *et al*. (2001b) Fire, climate change and fuel management in the Canadian boreal forest. *International Journal of Wildland Fire*, **10**, 405–413.

Amiro BD, Todd JM, Logan KA *et al*. (2001a) Direct Carbon emissions from Canadian forest fire, 1959 to 1999. *Journal of Forest Research*, **31**, 512–525.

Anderson IP, Imanda ID, Muhnandar (2000) *Vegetation Fires in Sumatra, Indonesia: Reflection on the 1999 Fires*. Forest fire prevention and Control Project, Palembag. European Union and Ministry of Forestry and Estate Crops, Jakarta, Indonesia.

Andreae MO (1991) Biomass burning: its history, use, and distribution and its impact on environmental quality and global climate. In: *Global Biomass Burning, Atmospheric, Climatic and Biosphere Implication* (ed. Levine JS), pp. 3–21. MIT Press, Cambridge, MA.

Arino O, Simon M, Piccolini I *et al*. (2001) *The ERS-2 ATSR-2 World Fire Atlas and the ERS-2 ATSR-2 World Burnt Surface Atlas Projects*. Proceedings 8th ISPRS conference on Physical Measurement and Signatures in Remote Sensing, Aussois, 8–12 January 2001.

Barbosa PM, Gregoire JM, Pereira JMC (1999b) An algorithm for extracting burned areas from time series of AVHRR GAC data applied at a continental scale. *Remote Sensing of Environment*, **69**, 253–263.

Barbosa PM, Pereira JMC, Gregoire JM (1998) Compositing criteria for burned area assessment using multitemporal low resolution satellite data. *Remote Sensing of Environment*, **65**, 38–49.

Barbosa PM, Stroppiana D, Gregoire JM (1999a) An assessment of vegetation fire in Africa (1981–1991). Burnt areas, burnt biomass and atmospheric emissions. *International Journal of Global Biogeochemical Cycles*, **13**, 933–950.

Bartlein PJ, Hostetler SW, Shafer SL *et al*. (2003) *The seasonal cycle of wildfire and climate in the western United States*. Preprints, 2nd International Wildland Fire Ecology and Fire Management Congress, and 5th Symposium on Fire and Forest Meteorology American Meteorological Society, 16–20 November 2003, Orlando, FL, Paper P3.9

Belward AS, Gregoire JM, D'Souza G *et al*. (1993) *In-situ, real-time fire detection using NOAA/AVHRR data*, Proceedings of the 6th AVHRR data users' meeting, Belgirate, Italy, 28th June–2nd July, 1993, EUMETSAT, Darmstadt, pp. 333–339.

Boles SH, Verbyla DL (2000) Comparison of three AVHRR-based fire detection algorithms for interior Alaska. *Remote Sensing of Environment*, **72**, 1–16.

Brest C, Rossow WR (1992) Radiometric calibration and monitoring of NOAA AVHRR data for ISCCP. *International Journal of Remote Sensing*, **13**, 235–273.

Brockett BH, Biggs HC, van Wilgen BW (2001) A patch mosaic burning system for conservation areas in southern African savannas. *International Journal of Wildland Fire*, **10**, 169–183.

Cahoon DR Jr, Levine JS, Cofer WR III *et al*. (1991) The great Chinese fire of 1987: a view from space. In: *Global Biomass Burning: Atmospheric, Climatic and Biospheric Implications* (ed. Levine JS), pp. 61–65. The MIT Press, Cambridge, MA.

Cahoon DR Jr., Stocks BJ, Levine JS *et al*. (1996) Monitoring the 1992 forest fires in the boreal ecosystem using NOAA AVHRR satellite imagery. In: *Biomass Burning and Climate Change – Vol. 2 – Biomass Burning in South America, Southeast Asia, and Temperate and Boreal Ecosystems, and the Oil Fires of Kuwait* (ed. Levine JL), pp. 795–802. MIT Press, Cambridge, MA.

Calvin M, Wettlaufer D (2000) Fires in the Southern Cape Peninsula, Western Cape Province, South Africa January 2000. *International Forest Fire News*, **22**, 69–75.

Camberlin P, Janicot S, Poccard I (2001) Seasonality and atmospheric dynamics of the teleconnection between African rainfall and tropical ocean surface temperature: Atlantic vs. ENSO. *International Journal of Climatology*, **21**, 973–1005.

Christopher SA, Wang M, Berendes TA *et al*. (1998) The 1985 biomass burning season in South America: satellite remote sensing of fires, smoke, and regional radiative energy budgets. *Journal of Applied Meteorology*, **37**, 661–678.

Cihlar JJ, Li CZ, Huang F *et al*. (1998) Can interannual land surface signal be discerned in composite AVHRR data? *Journal of Geophysical Research*, **103**, 23163–23172.

Conard SG, Ivanova GA (1998) Wildfire in Russian boreal forests – potential impacts of fire regime characteristics on emissions and global carbon balance estimates. *Environmental Pollution*, **98**, 305–313.

Conard SG, Sukhinin AI, Stocks BJ *et al*. (2002) Determining effects of area burned and fire severity on carbon cycling and emissions in Siberia. *Climatic Change*, **55**, 197–211.

Craig R, Heath B, Raisbeck-Brown N *et al*. (2002) The distribution, extent and seasonality of large fires in Australia, April 1998–March 2000, as mapped from NOAA–AVHRR imagery. In: *Australian Fire Regimes: Contemporary Patterns (April 1998–March 2000) and Changes since European Settlement, Australia State of the Environment Second Technical Paper Series (Biodiversity)* (eds Russell-Smith J, Craig R, Gill AM, Smith R, Williams J), Department of the Environment and Heritage, Canberra (http://www.ea.gov.au/soe/techpapers/index.html).

Crutzen PJ, Carmichael GR (1993) Modeling the influence of fires on atmospheric chemistry. In: *Fire in the Environment: Its Ecological, Climatic and Atmospheric Chemical Importance* (ed. Goldammer JG), Wiley, John & Sons, Incorporated, NY.

Crutzen PJ, Heidt LE, Krasnec JP *et al*. (1979) Biomass burning as a source of atmospheric gases CO, H_2, N_2O, NO, CH_3Cl and COS. *Nature*, **282**, 253–256.

Cwielong P (1996) The 1995–1996 Wildfire Season in Patagonia. *International Forest Fire News*, **15**, 22–23.

Cwielong P, Rodriguez N (1993) Forest fire research in the Patagonia Region, Argentina –'Andino Patagonico'. *International Forest Fire News*, **9**, 2–5.

Davies D, Kumar S, Descloitres J (2004) Global fire monitoring using MODIS near-real-time satellite data. *GIM International*, **18**, 41–43.

De Fries RS, Hansen M, Townshend JRG *et al*. (1998) Global land cover classifications at 8 km spatial resolution: the use of training data derived from landsat imagery in decision trees classifiers. *International Journal of Remote Sensing*, **19**, 3141–3168.

Delmas R, Loudjani P, Podaire A *et al*. (1991) Biomass burning in Africa: an assessment of annually burnt biomass. In: *Global Biomass Burning* (ed. Levine JS), pp. 126–133. MIT Press, Cambridge, MA.

Dignon J, Penner JE (1991) Biomass burning: a source of nitrogen oxides in the atmosphere. In: *Global Biomass Burning* (ed. Levine JS), pp. 370–375. MIT press, Cambridge, MA.

Dube P (2004) Personal communication, Department of Environmental Science. University of Botswana.

Duncan BN, Martin RV, Staudt AC *et al*. (2003) Interannual and seasonal variability of biomass burning emissions constrained by satellite observations. *Journal of Geophysical Research*, **108**, 4100 (doi: 10.1029/2002JD002378).

Dwyer E, Pinnok S, Gregoire J-M *et al*. (2000) Global spatial and temporal distribution of vegetation fire as determined from satellite observations. *International Journal of Remote Sensing*, **21**, 1289–1302.

Edwards AC, Hauser P, Anderson M *et al*. (2001) A tale of two parks: contempary fire regimes of Litchfield and Nitmiluk National Parks, monsoonal northern Australia. *International Journal of Wildland Fire*, **10**, 79–89.

Elvidge CD, Hobson VR, Baugh KE *et al*. (2001) DMSP–OLS estimation of tropical forest area impacted by surface fires in Roraima, Brazil: 1995 versus 1998. *International Journal of Remote Sensing*, **22**, 2661–2673.

Erdenesaikhan N, Erdenetuya M (1999) Forest and steppe fire monitoring in Mongolia using satellite remote sensing. *International Forest Fire News*, **21**, 71–74.

Eva H, Lambin EF (1998) Burnt area mapping in Central Africa using ATSR data. *International Journal of Remote Sensing*, **19**, 3473–3497.

FAO (2001a) *FRA Global Forest Fire Assessment 1990–2000*. Forest Resources Assessment Programme, Working Paper 55. FAO, Rome.

FAO (2001b) *FRA Global Forest Resources Assessment 2000*. Main Report. Forest Resources Assessment Programme, FAO Forestry paper 140, Rome.

Galanter M, Levy HII, Carmichael GR (2000) Impacts of biomass burning on tropospheric CO, NO_x and O_3. *Journal of Geophysical Research*, **105**, 6633–6653.

Galindo I, López-Pérez P, Evangelista-Salazar M (2003) Real-time AVHRR forest detection in Mexico (1998–2000). *International Journal of Remote Sensing*, **24**, 9–22.

GCOS (2003) *The second report on the adequacy of the global observing systems for Climate in support of the UNFCCC*, April 2003, GCOS-82, WMO Technical Document 1143, WMO, Geneva, 74 pp.

Goldammer JG (ed.) (1992) *Tropical Forest in Transition: Ecology of Natural and Anthropogenic Disturbance Processes: An Introduction*, **Vol. 1**. Birhauser-Verlag, Basel, Boston.

Goldammer JG, Hoffmann AA (2001) *'Fire situation in Indonesia' in 'FRA 2000. Global Forest Fire Assessment, 1990–2000'. Forest Resources Assessment Programme*. Forestry Department. FAO Working Paper 55, Rome, pp. 132–144.

Gordon HR, Brown JW, Evans RH (1988) Exact Rayleigh scattering calculations for use with the Nimbus-7 coastal colour scanner. *Applied Optics*, **27**, 2111–2122.

Guenther BW, Butler J, Ardanuy P (1997) *Workshop on Strategies for Calibration and Validation of Global Change Measurements. May 10–12, 1995, NASA Reference Publication 139*. NASA/GSFC, Greenbelt, MD, USA.

Gutman GG (1999) On the monitoring of land surface temperatures with the NOAA/AVHRR: removing the effect of satellite orbit drift. *International Journal of Remote Sensing*, **20**, 3407–3413.

Hao WM, Liu MH (1994) Spatial and temporal distribution of tropical biomass burning. *Global Biogeochemical Cycles*, **8**, 495–503.

Hicke JA, Asner GP, Kasischke ES *et al*. (2003) Post Fire response of North American boreal Forest net primary productivity analyzed with satellite observations. *Global Change Biology*, **9**, 1145–1157.

Huggard CJ, Gomez AR (2001) *Forest Under Fire: A Century of Ecosystem Mismanagement in the Southwest*. University of Arizona Press, Tucson.

IPCC (2000) *Land Use, Land Use Change, and Forestry*. Cambridge University Press, Cambridge, UK.

Isaaks E, Srivastava M (1989) *An Introduction to Applied Geostatistics. ISBN 0-19-505013-4*. Oxford University Press, New York.

Jaiswal RK, Mukherjee S, Raju KD *et al*. (2002) Forest fire risk zone mapping from satellite imagery and GIS. *International Journal of Applied Earth Observation and Geoinformation*, **4**, 1–10.

James ME, Kalluri SNV (1994) The pathfinder AVHRR land data set: an improved coarse resolution data set for terrestrial monitoring. *International Journal of Remote Sensing*, **15**, 3347–3363.

Johnston T (1999) Canada Report 1998. *International Forest Fire News*, **20**, 40–45.

Justice CO, Giglio L, Korontzi S *et al*. (2002) The MODIS fire products. *Remote Sensing of Environment*, **83**, 244–262.

Kasischke ES, Morrissey L, Way JB *et al*. (1995) Monitoring seasonal variations in boreal ecosystems using multi-temporal spaceborne SAR data. *Canadian Journal of Remote Sensing*, **21**, 96–109.

Kaufman YJ, Remer LA (1994) Detection of Forests using Mid-IR reflectance: an application for aerosol studies. *IEEE Transactions on Geoscience and Remote Sensing*, **32**, 672–683.

Kidwell KD (1995) *NOAA Polar Orbiter Data User's Guide*, US Department of Commerce, National Oceanic and Atmospheric Administration, National Environmental Satellite, Data and Information Service (NOAA/NESDIS) 1995. Available on the web at: http://www2.ncdc.noaa.gov/docs/podug/cover.htm).

Legg CA, Laumonier Y (1999) Fires in Indonesia, 1997: a remote sensing perspective. *Ambio*, **28**, 479–485.

Li Z, Nadon S, Cihlar J (2000) Satellite detection of Canadian boreal forest fires: development and application of the algorithm. *International Journal of Remote Sensing*, **21**, 3057–3069.

Lyon B (2004) The strength of El Niño and the spatial extent of tropical drought. *Geophysical Research Letters*, **31**, L21204 (doi: 10.1029/2004GL020901).

Malingreau JP, Stephens G, Fellows L (1985) Remote sensing of forest fires: Kalimantan and North Borneo in 1982–83. *Ambio*, **14**, 314–321.

Manzo-Delgado L, Aguirre-Gómez R, Alvarez R (2004) Multitemporal analysis of land surface temperature using NOAA–AVHRR: preliminary relationships between climatic anomalies and forest fires. *International Journal of Remote Sensing*, **25**, 4417–4424.

McKenzie D, Bayard AK, Kopper KE *et al*. (2004) *A rule-based classification of fuels for landscape modeling of fire (qualitative coarse-scale mapping of fuels across western US using USFS FERA's FCCS system)*. Ecological Society of America Meeting, August 1–6, 2004.

Moreno-Ruiz JA, Barbosa PM, Carmona-Moreno C *et al*. (1999) *GLINTS-BS–global burn scar detection system*. European Union Technical Note I.99.167.

Oura B (1999) Management and prevention of forest fires in Côte d'Ivoire SODEFOR's forest fire protection programme. *International Forest Fire News*, **20**, 50–56.

Payette S (1992) Fire as a controlling process in the North American boreal forest. In: *A Systems Analysis of the Global Boreal Forest* (ed. Shugart HH, Leemans R, Bonan GB), Cambridge University Press, Cambridge.

Pereira JMC, Dos Santos MTN (2003) *Forest Risk and Burned Area Mapping in Portugal, ISBN 972-8097-50-6*. Direccao-Geral das Forestas, Lisboa.

Pinty B, Verstraete MM (1992) GEMI: a non-linear index to monitor global vegetation from satellite. *Vegetatio*, **101**, 1335–1372.

Potter C, Tan PN, Steinbach M *et al*. (2003) Major disturbance events in terrestrial ecosystems detected using global satellite data sets. *Global Change Biology*, **9**, 1005–1021.

Price JC (1991) Timing of NOAA afternoon passes. *International Journal of Remote Sensing*, **12**, 193–198.

Rao CRN, Chen J, Staylor FW *et al*. (1993) *Degradation of the visible and near-infrared channels of the Advanced Very High Resolution Radiometer on the NOAA-9 spacecraft: assessment and recommendations for corrections*. NOAA Technical Report NESDIS-70. NOAA/NESDIS, Washington, DC.

Reddy MS, Venkataraman C (2002) Inventory of aerosol and sulphur dioxide emissions from India. Part II – biomass combustion. *Atmospheric Environment*, **36**, 699–712.

Rodo X, Baert E, Comin FA (1997) Variations in seasonal rainfall in Southern Europe during the present century: relationships with the North Atlantic Oscillation and the El Niño-Southern Oscillation. *Climate Dynamics*, **13**, 275–284.

Romme WH, Despain DG (1989) Historical perspective on the Yellowstone Fires of 1988. *Bioscience*, **39**, 696–699.

Rorig ML, Ferguson SA (1999) Characteristics of lightning and wildland fire ignition in the Pacific Northwest. *Journal of Applied Meteorology*, **38**, 1565–1575.

Russell-Smith J, Yates C, Edwards A *et al*. (2003) Contemporary fire regimes of northern Australia, 1997–2001: change since Aboriginal occupancy, challenges for sustainable management. *International Journal of Wildland Fire*, **12**, 283–297.

Saha S, Hiremath A (2003) Anthropogenic fires in India: a tale of two forests. *Arid Lands Newsletter*, **54**. Also available at http://ag.arizona.edu/OALS/ALN/aln54/saha.html

Seiler W, Crutzen PJ (1980) Estimates of gross and net fluxes of carbon between the biosphere and the atmosphere from biomass burning. *Climatic Change*, **2**, 207–247.

Self S, Zhao JX, Holasek RE *et al*. (1996) *The Atmospheric Impact of the 1991 Mount Pinatubo Eruption in FIRE and MUD: Eruptions and Lahars of Mount Pinatubo, Philippines*. University of Washington Press, Seattle, WA.

Shulman D (1996) Wildfires in Mongolia 1996. *International Forest Fire News*, **15**, 30–35.

Siegert F, Ruecker G, Hinrichs A *et al*. (2001) Increased damage from fires in logged forests during droughts caused by El Niño. *Nature*, **414**, 437–440.

Soja AJ, Sukhinin AI, Cahoon DR Jr *et al*. (2004) AVHRR-derived fire frequency, distribution and area burned in Siberia. *International Journal of Remote Sensing*, **25**, 1939–1960.

Stocks BJ (1991) The extent and impact of forest fires in northern circumpolar countries. In: *Global Biomass Burning: Atmospheric, Climatic, and Biospheric Implications* (ed. Levine JS), pp. 197–202. MIT Press, Cambridge, MA.

Swetnam TW, Betancourt JL (1990) Fire-southern oscillation relations in the Southwestern United States. *Science*, **249**, 1017–1020.

Swetnam TW, Allen CD, Betancourt JL (1990) Applied historical ecology: using the past to manage for the future. *Ecological Applications*, **9**, 1189–1206.

Tanimoto H, Kajii Y, Hirokawa J *et al*. (2000) The atmospheric impact of boreal forest fires in far eastern Siberia on the seasonal variation of carbon monoxide: observations at Rishiri, a northern remote island in Japan. *Geophysical Research Letters*, **27**, 4073–4076.

Tansey K, Grégoire J-M, Stroppiana D *et al*. (2004) Vegetation burning in the year 2000: global burned area estimates from SPOT VEGETATION data. *Journal of Geophysical Research – Atmospheres*, **109**, D14S03, (doi: 10.1029/2003JD003598).

Taylor RV (1990) *Implementation of reflectance models in operational AVHRR radiation budget processing*. NASA Technical Report NESDIS – 49, NOAA, Boulder, CO.

Tilman D, Reich P, Phillips H *et al*. (2000) Fire suppression and ecosystem carbon storage. *Ecology*, **81**, 2680–2685.

Thonicke K, Venevsky S, Sitch S *et al*. (2001) The role of fire disturbance for global vegetation dynamics: coupling fire into a dynamic global vegetation model. *Global Ecology and Biogeography*, **10**, 661–677.

Williams J (2001) *Biodiversity issues and challenges*. Australia State of the Environment Report 2001 (Theme Report). CSIRO Publishing on behalf of the department of the Environment and Heritage, 2001.

Wooster MJ, Ceccato P, Flasse SP (1998) Indonesian fires observed using AVHRR. *International Journal of Remote Sensing*, **19**, 383–386.

Wooster MJ, Strub N (2000) Study of the 1997 borneo fires: quantitative analysis using Global Area Coverage (GAC) satellite data. *Global Biogeochemical Cycles*, **16**, 1–12.